Fabrication of Redox- Responsive Doxorubicin and Paclitaxel Prodrug Nanoparticles with Microfluidics for Selective Cancer Therapy

Xiaodong Ma,[a,b] Ezgi Özliseli,[b] Yuezhou Zhang,*[b] Guoqing Pan,[c] Dongqing Wang,*[a] and Hongbo Zhang,*[a,b,d]

Cancer is an exceptionally confounded disease that demands to develop powerful drug/drugs, without inducing heavy adverse drug effects. Thus, different approaches have been applied to improve the targeted delivery of cancer drugs, for example by using nanocarriers. However, the nanocarriers are foreign materials, that needs further validation for their biocompatibility and biodegradability. In this study, we have chemically conjugated hydrophilic anticancer drug doxorubicin (DOX) with hydrophobic drug Paclitaxel (PTX) through a redox-sensitive disulfide bond, abbreviated as DOX-S-S-PTX. Subsequently, due to the amphiphilic characterization, the prodrug can self-assemble into nanoparticles under microfluidic nanoprecipitation. This novel prodrug nanoparticle has super high drug loading degree of 89%, which is impossible to achieve by any nanocarrier systems, and can be tailored to 180 nm to deliver themselves to the target, and release DOX and PTX under redox condition, which is often found in cancer cells. By evaluating the cell viability in MDA-MB-231, MDA-MB-231/ADR and MEF cell lines, we observed that the prodrug nanoparticles effectively killed the cancer cells, and conquered the MDA-MB-231/ADR selective. Meanwhile, MEF cells were spared due to the lacking of redox condition. The cell interaction results show that the reduced intermediate of prodrug can also bind to parent drugs biological targets. The hemolysis results show that the nanoparticles are biocompatible in blood. The computer modelling suggested that the prodrug is unlikely to bind to biological targets that parent drugs still strongly interact with. At last, we confirm that the prodrug nanoparticles have no therapeutic effect in blood and healthy cells, but can selectively eliminate the cancer cells that meet the redox condition to cleave the disulfide bond and release the drugs DOX and PTX.

1. Introduction

Cancer is globally the second leading disease of mortality,[1, 2] nearly 1 in 6 deaths is ascribed to cancer. It can occur at any stage of life without gender and racial exclusion, even in wildlife.[3] Hence, the battle against cancer is always on. Among versatile treatments, chemotherapy might be the most important option for most cancers because of its high efficiency. However, unlike surgery or radiation which target specific areas, conventional chemotherapy works throughout the human body. Such indistinguishable administer process will inevitably attack healthy cells unless the drug itself is a target-selective.[4] Breast cancer accounts for the second leading cause of cancer-related mortality among women worldwide.[5]

Prodrugs are compounds bearing little or no pharmacological activity, after administration, metabolized to the active daughter drug through the enzymatic/chemical process. Prodrugs have been experienced to be discovered by chance or being designed on purpose. Such efforts are trying confront drug development hurdles that limit formulation options or result in unwanted performances, or off-targeting effects.[6] It is also an approach to address bioavailability of the low aqueous solubility drug, in which the native hydrophobic drug is masked into a hydrophilic form that can be converted by endogenous enzymes[7, 8] to the native drug, have been utilized to “redeem” water-insoluble drug candidates or to improve the availability of existing drugs. Since the past decade, more than 30 prodrugs have been marketed.[6]

"Nanotech" is technology to understand or manipulate matter at the scale about 1 to 100 nanometers where unique properties offer novel applications.[9] Drug delivery and release through nanotechnology have emerged as a promising approach for a number of drug or drug candidates to give satisfied outcomes.[10] Drug nanoparticle can be prepared through a variety of protocols, exemplified by emulsion-solvent evaporation,[11] double emulsion and evaporation,[12] emulsions-diffusion,[13] salting out[14] and solvent displacement method.[15, 16] Solvent displacement involves the diffusion of the organic solvent in the aqueous medium in the presence of a surfactant. Drug and the surfactant are dissolved in a water-miscible mixture with an aqueous solution under magnetic stirring. As a result, nanoparticles are formed instantaneously by the rapid solvent diffusion. It was observed that the mixing of the organic phase into the aqueous phase heavily affect the particles size and polydispersity. For the bulk method, often the organic solution is poured into aqueous medium or stepwise added without precise control of organic phase. Therefore, give rise to physicochemical unsatisfied particles. However, microfluidics-based technology is more controllable and has been widely used for drug loading and delivery related nanoassemblies.[17, 18] The application of this approach to fabricate drug nanocrystals has been showed as not only the proof-of-concept,[19] but held great potential to scale-up, especially for nanoprecipitation of poorly water-soluble anticancer drugs Paclitaxel(PTX) and Sulforaphane (SFN).[20]

However, due to the instability of those drug crystals, the obtained drug nanocrystal was further encapsulated with a polymer to give core/shell structures and give 42.6% (PTX) and 45.2%(SFN) of drug loading by using the superfast sequential nanoprecipitation method.[20]

The combination of nanoprecipitation with prodrug seems to be an effective approach to tackle unmet therapeutic need. For instance, "squalenoylation" of antiretroviral compounds dideoxycytidine and didanosine that spontaneously self-organize in water as stable nanoassemblies has already been applied to the intravenous administration.[21] Gaudin et al also conjugated adenosine to the lipid squalene and subsequently formatted squalenoyl adenosine prodrug into nanoassemblies offered prolonged circulation of the nucleoside, providing neuroprotection in mouse stroke and rat spinal cord injury models both in vitro and in vivo studies.[22] In this prodrug conjugation, squalenoyl functioned as the lipid nanocarrier to balance the hydrophilicity of adenosine but have no therapeutic contributions, resulting in 37% drug loading. The drug loading, in theory, could be as high as 100% if the two therapeutic drugs can be covalently conjugated together without using of any linker in between. For example, hydrophilic anticancer drug irinotecan(Ir) and the hydrophobic anticancer drug chlorambucil(Cb) were jointed together through via an ester bond which formed from the hydroxyl group of Ir and the carboxylic acid group of Cb.[23] It is clear that the selection of drugs for conjugate will never be arbitrary.

To fully fulfill the advantage of prodrug and facilitate subsequent nanoprecipitation, several principles should be taken into account: 1) feasibility of covalent conjugation, which means the components need to bear suitable functional group to enable the chemical reaction occurred; 2) synergism of candidate to specific biological targets is always pursued or at least has no side effects while antagonism must be avoided; 3) the balance of hydrophobicity and hydrophilicity, the bias of either side will impair the formation of the desired nanoparticle; 4) the fragileness of prodrug in biological microenvironment, requiring the input prodrug have to be fragmented; 5) the possibility to monitor pharmacokinetics of processed prodrug particles. Following the above-mentioned know-how, we choose DOX and PTX as monomer to synthesize drug conjugate based on the following reasons: 1) DOX and PTX are synergistic in breast cancer cell;[24] 2) both amine group of DOX and hydroxyl group of PTX can react with carboxylic acid, indicating a linker with bi-carboxylic acid functional group is needed to join them together; 3) DOX is hydrophilic while PTX is hydrophobic; the coupling of the two drugs result in an amphiphilic molecule; 4) 3,3'-dithiodipropionic acid contains disulfide bond which is reduced reagent breakable. Reduced glutathione (L-γ-glutamyl-L-cysteinyl-glycine; GSH) level is 100 times higher In cancer cells than in normal ones,[25] therefore, is a biomarker of disease cell and prodrug destructor. 5) DOX is known to be fluorescent hence can be monitored by using spectroscopy instrument. As illustrated in Fig. 1, we have conjugated DOX with PTX with a redox-sensitive linker and subsequently precipitated the prodrug to nanoparticles (NPs) with microfluidics. The effect and selectivity of those prodrug nanoparticles on cancer cells are evaluated with breast cancer cell lines MDA-MB-231, MDA-MB-231/ADR and Mouse embryonic fibroblasts (MEF). As a proof-of-concept, we hypothesize the prepared NPs will selectively internalize and accumulated into cancer tissue attributed to EPR effects.[26]

2. EXPERIMENTAL

2.1 Materials

Doxorubicin (DOX) and Paclitaxel (PTX) were purchased from Arisun ChemPharm Co., Ltd (China). 3,3'-dithiodipropionic acid (DTDP), 4-dime-thylaminopyridine (DMAP) and N-(3-Dimethylaminopropyl)-N-ethylcarbodiimide hydrochloride (EDC.HCl) were purchased from Alfa Aesar (Finland). DL-dithiothreitol (DTT), acetyl chloride, N, N-dimethylformamide (DMF), triethylamine (TEA), dichloromethane (DCM), Menthol (MeOH) were purchased from Sigma-Aldrich (Finland). Cellulose ester membranes (dialysis bag) with a molecular weight cut-off value (MWCO) of 3500 were purchased from Solarbio.com, Beijing, China.

2.2. Synthesis and characterization of DOX-S-S-PTX

As shown in Figure 2, the amphiphilic DOX-S-S-PTX prodrug conjugate was synthesized through esterification and amide coupling reaction.

2.2.1. Synthesis of dithiodipropionic anhydride (DTDPA)

DTDPA was obtained by acylation of 3,3'-Dithiodipropionic acid(DTPA) with acetyl chloride according to the previous literature.[27] Briefly, DTPA (3.0 g, 48 mmol) was dissolved in acetyl chloride (30 mL) and refluxed at 70 °C for 12 h. After the

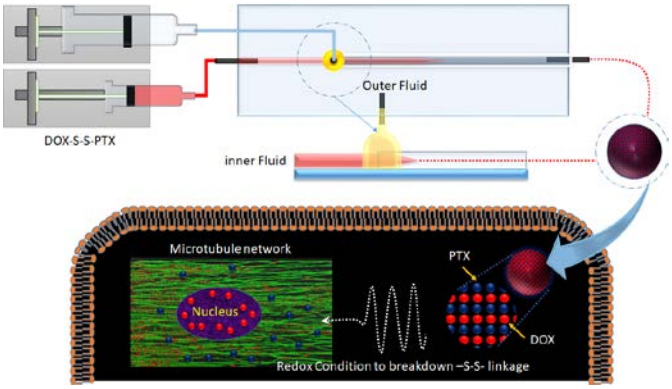

Fig. 1. Illustration of DOX-S-S-PTX nanoparticle for breast cancer cell

solvent was removed, the residue was precipitated into excess ethyl ether to afford DTDPA and vacuum-dried (2.7 g, 90%) as white solid. 1H NMR (400 MHz, DMSO-d6): δ ^{1}H NMR (500 MHz, DMSO-d6) δ 2.87 (t, J = 6.9 Hz, 4H), 2.61 (t, J = 6.9 Hz, 4H).

2.2.2 Synthesis of PTX-S-S-COOH

PTX derivative PTX-S-S-COOH was synthesized through esterification.[28] In brief, PTX (1.0 g, 1.17 mmol), DTDPA (270.2 mg, 1.41 mmol), TEA (142.2 mg, 191.7 µl) and DMAP (28.61 mg, 0.23 mmol) were dissolved in 20 ml methylene chloride. The mixture was stirred at room temperature overnight. Upon the completion of the reaction monitored by LCMS until the starting material vanished. Then, the crude product was purified by silica gel column chromatography to obtain the pure intermediate (yield = 88%). 1H NMR (400 MHz, DMSO-d_6): δ ^{1}H NMR (500 MHz, DMSO-d6) δ 1H NMR (500 MHz, DMSO-d6) δ 9.48 (d, J = 7.1 Hz, 1H), 7.98 (d, J = 7.2 Hz, 2H), 7.88 (d, J = 7.1 Hz, 2H), 7.73 (d, J = 6.9 Hz, 1H), 7.67 (d, J = 7.3 Hz, 2H), 7.54 (d, J = 7.0 Hz, 1H), 7.45 (d, J = 7.3 Hz, 4H), 7.19 (d, J = 6.3 Hz, 1H), 6.30 (s, 1H), 5.81 (t, J = 8.1 Hz, 1H), 5.56 (t, J = 8.6 Hz, 1H), 5.41 (t, J = 7.7 Hz, 2H), 4.91 (d, J = 9.0 Hz, 1H), 4.66 (s, 1H), 4.14–4.09 (m, 1H), 4.01 (s, 2H), 3.61–3.56 (m, 2H), 2.95–2.74 (m, 8H), 2.35 (s, 1H), 2.25 (s, 3H), 2.10 (s, 3H), 1.79 (s, 3H), 1.72-1.57 (m, 2H), 1.50 (s, 3H), 1.23 (s, 1H), 1.01 (d, J = 15.1 Hz, 5H). HRMS (ES-) for $C_{53}H_{58}NO_{17}S_2$ $[M-H]^-$ calculated 1044.3152, found 1044.3259 (Fig. S3). HRMS [2M] calculated 2090.6449, found 2090.6547.

2.2.3 Synthesis of PTX-S-S-DOX

PTX-S-S-DOX was synthesized through amide coupling. Briefly, DOX.HCl (77.93 mg, 0.14 mmol), PTX-S-S-COOH (100 mg, 0.1 mmol) EDC.HCl (27.49 mg, 0.14 mg) and TEA (14.51 ml, 19.55 µl) were dissolved in DMSO and protected with aluminium foil from light. The reaction mixture was stirred at room temperature overnight, then DMSO was removed by lyophilisation. The residues were purified by silica gel column chromatography (MeOH-CH_2Cl_2) to obtain the pure products to obtain a red powder (yield 56%). δ ^{1}H NMR (500 MHz, Chloroform-d) δ 13.90 (s, 1H), 13.16 (s, 1H), 8.10 (d, J = 7.2 Hz, 2H), 7.96 (d, J = 7.4 Hz, 1H), 7.74 (d, J = 8.2 Hz, 1H), 7.72 (d, J = 7.2 Hz, 2H), 7.60 (t, J = 7.4 Hz, 1H), 7.50 (t, J = 7.7 Hz, 2H), 7.43 (t, J = 7.4 Hz, 1H), 7.37-7.33 (m, 8H), 6.31 (d, J = 8.4 Hz, 1H), 6.28 (s, 1H), 6.15 (t, J = 8.6 Hz, 1H), 5.90 Hz, 1H), 5.43 (s, 1H), 5.21 (s, 1H), 4.70 (s, 2H), 4.39

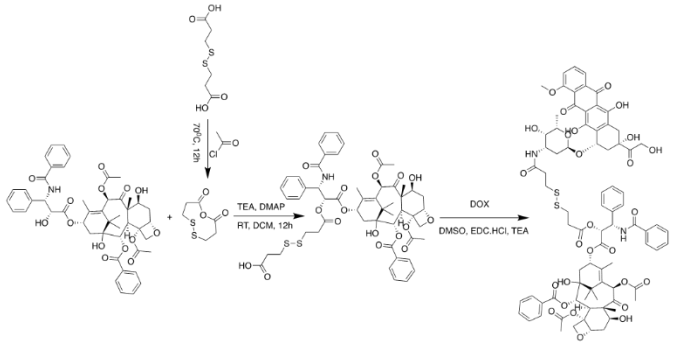

Fig. 2. Synthesis route of DOX-S-S-PTX

(dd, J = 10.7, 6.8 Hz, 1H), 4.28 (d, J = 8.4 Hz, 1H), 4.17 (d, J = 8.5 Hz, 1H), 4.11 (d, J = 6.5 Hz, 2H), 4.02 (s, 3H), 3.76 (d, J = 7.0 Hz, 1H), 3.58 (s, 1H), 3.19 (d, J = 18.6 Hz, 1H), 2.93 (d, J = 18.7 Hz, 1H), 2.88–2.69 (m, 8H), 2.54–2.44 (m, 2H), 2.39 (s, 3H), 2.33–2.23 (m, 3H), 2.20 (s, 3H), 2.13–2.04 (m, 3H), 1.88 (s, 3H), 1.77 (d, J = 7.7 Hz, 2H), 1.65 (s, 3H), 1.24 (d, J = 6.3 Hz, 4H), 1.19 (s, 3H), 1.12 (s, 3H). HRMS (ES+) for $C_{80}H_{86}N_2O_{27}S_2$ $[M+Na]^+$ calculated 1593.4757, found 1593.4638 (Fig. S3).

2.2.4. Characterization of the prodrug

The ^{1}H NMR spectra of DTDP, DTDPA, DOX, PTX, PTX-S-S-COOH and DOX-S-S-PTX were recorded on Bruker 500 NMR spectrometers (Bruker, Billerica, MA, USA) and chemical shifts (δ, ppm) are quoted relative to the residual solvent peak (Chemical shifts (δ, ppm) are reported relative to the solvent peak ($CDCl_3$, 7.26 [^{1}H]; DMSO-d_6, 2.50 [^{1}H]). Mass spectra were recorded on a Bruker Daltonics microTOF-Q mass spectrometer (Bruker, Billerica, MA, USA). In addition, the FTIR spectra of DOX, PTX, PTX-S-S-COOH and DOX-S-S-PTX were recorded on a Thermo Scientific Nicolet iS50 Fourier transform infrared spectrometer in the wavenumber of 400-4000 cm^{-1}.

2.3. Fabrication of three-dimensional (3D) microfluidic devices

The 3D microfluidic co-flow focusing device was fabricated by assembling two (inner and outer) borosilicate glass capillaries on a glass slide.[29] One end of the cylindrical capillary (an outer diameter of around 1000 µm; World Precision Instruments Ltd., UK) was tapered using a magnetic glass microelectrode horizontal needle puller (P-31, Narishige Co.,Ltd, Japan). The inner tapered capillary was polished until the cross-section of the shape and end remained flattened using sandpaper (Indasa Rhynowet, Portugal). The inner tapered capillary was inserted into another cylindrical capillary with an inner dimension of around 1100 µm (World Precision Instruments Ltd., UK), and coaxially aligned. A transparent epoxy resin (5 Minute® Epoxy, Devcon) was used to seal the capillaries when required.

2.4. Preparation of nanoparticles

We firstly prepared the prodrug particle using bulk method. In detail the ethanolic prodrug solution was dropwise added into water with surfactant, followed by centrifuge to remove ethanol and resuspend the particles. By comparison, the DOX-S-S-PTX nanoparticles were also prepared by our in-house microfluidics devices.[30, 31] Two miscible liquids (aqueous and methanol) were injected separately into the microfluidic device through polyethylene tubes connected to syringes by needle at constant flow rates. The flow rate of the different liquids was controlled by pumps (PHD 2000, Harvard Apparatus, USA). The DOX-S-S-PTX in methanol (5 mg/mL) served as the inner dispersed phase; meanwhile, a Pluronic® F-127 (Sigma-Aldrich, Finland), 0.1% aqueous solution was selected as the outer continuous fluid. The inner (2 mL/h) and outer (40 mL/h) fluids were separately pumped into the microfluidic device, in which the inner fluid was focused by the outer continuous fluid. In this procedure, water amphiphilic DOX-S-S-PTX self-assembled into the nanoparticles during diffusion from the ethanol solution into water, and thus, the bare DOX-S-S-PTX nanoparticles were obtained. In order to optimize the physicochemical properties of the prepared nanoparticles, including particle size, polydispersity index (PDI) and zeta (z)-potential, several process variables and formulation parameters were evaluated, such as the flow ratio between the inner and outer fluids and the concentration of DOX-S-S-PTX.

2.5. Characterization of the nanoparticles

Particle sizing was performed using dynamic light scattering with Zetasizer Nano ZS (Malvern Instruments Ltd., UK). For each measurement, the sample (1.0 mL) was put in a disposable polystyrene cuvette (SARSTEDT AG & Co., Germany). The nanocarrier surface ζ-potential was measured with Zetasizer Nano ZS by using disposable folded capillary cells (DTS1070, Malvern, UK). Both the size and ζ-potential were recorded as the average of three measurements. The structure of the fabricated nanoparticle was evaluated by transmission electron microscope (TEM; JEOL 1400 Plus, JEOL, USA) at an acceleration voltage of 120 kV. The TEM samples were prepared by depositing 10 µL of the nanoparticle suspensions (1.0 mg/mL) onto carbon coated copper grids (200 mesh; Ted Pella, Inc., USA). Samples were blotted away after 5 min incubation then air-dried prior to imaging.

2.6. The in vitro release of DOX and PTX from the nanoparticles

The cumulative levels of DOX and PTX released from the DOX-S-S-PTX nanoparticles were characterized using the dialysis method.[32] In brief, 5 mL of PTX-loaded micellar solutions (1.0 mg/mL) in PBS (1X, pH 7.4, used except additional statement) were transferred into a dialysis membrane bag (MWCO 3500, Fisher Scientific), which were then immersed in 50 mL of PBS with or without DTT (10 mM), and suspended in a water bath at a constant temperature of 37 °C with horizontal shaking. Herein, DTT was used as a reducing agent to mimic the role of GSH which in microenvironment of cancer cells provide a reducing environment. At each predetermined time interval, 1 mL of incubated solution was taken out and replenished with an equal volume of corresponding PBS. The amount of PTX and DOX were all quantified by HPLC using an Agilent 1100 (Agilent Technologies, USA). PTX and DOX were simultaneously determined with a mobile phase composed of water and acetonitrile. The wavelengths used for PTX and DOX were 254 nm. The flow rate of mobile phase was 1.0 mL/min, the temperature was set at 30 °C, using a Waters Symmetry Shield RP18 Column (4.6 X 250 mm, 5 mm, Waters Corporation, USA) as the stationary phase, and the sample injection volume was 20 µL. A binary solvent system was used (solvent A, 0.1% aqueous TFA; solvent B, 0.1% TFA ACN), with UV detection by detector (UV-975, Jasco) at 254 nm. A gradient of 5-95% solvent B over 20 min for a 25 min run time was used.to first identify the retention time of parent drug (Fig. S1) then build up standard curves (Fig. S2) were established from known concentrations of PTX in ethanol solution and DOX in Milli-Q water.

2.7. Cell studies

2.7.1. Cell culture and maintenance

Triple negative breast cancer cell line MDA-MB-231, MDA-MB-231/ADR (MDA-MB-231 cell line with induced drug resistance by doxorubicin) and healthy cells mouse embryonic fibroblasts (MEF) were used for in vitro studies. The p-glycoprotein expression level of MDA-MB-231/ADR cells was confirmed (data not shown). The cells were cultured in high glucose Dulbecco's Modified Eagle medium (DMEM) supplemented with 10% FBS, 1% penicillin-streptomycin and 2 mM L-Glutamine at 37◦C, in a humidified incubator with 5% CO_2. Cells were passaged 2-3 times a week once they reach 90-100% confluency.

2.7.2 Cytotoxicity assay

WST-1 cell viability assay was used to determine drug efficacy in cancer and healthy cells. MDA-MB-231, MDA-MB-231/ADR cancer cells and MEF cells were incubated overnight in a 96-well-plate (7000 cells/well) in cell growth media at 37◦C with 5% CO_2. Following day, cell growth media was replaced with the fresh media containing 0.05, 0.1, 0.5, 1, 5 and 10 µM free drug or nanoparticle concentrations and incubated for 24h or 48h. Free drug stock solutions (DOX, PTX, DOX+PTX) were prepared in DMSO and nanoparticles (DOX-S-S-PTX) were suspended in water. All the dilutions for cell viability assay, including control, were prepared in cell growth media as DMSO concentration was 1%. After incubation with free drug or nanoparticles, 10 µL of WST-1 reagent was added to each well and cells were incubated for determined time (2h for cancer cells and 3h for fibroblasts) at 37◦C with 5% CO_2. After the incubation, absorbance was measured by Varioskan Flash Multimode Reader (Thermo Scientific Inc., Waltham, MA, USA) at 440 nm. Duplicates or triplicates were used for the experiment and averaged absorbance readings were plotted. To eliminate the background due to doxorubicin, absorbance values of cells without WST-1 reagent were measured and subtracted prior to the plotting.

2.7.3. Cellular uptake study

Cells were incubated overnight for attachment in 12 well plates ($15x10^4$ cells/well). DOX, PTX, DOX+PTX and DOX-S-S-PTX NPs were incubated with cells to keep the final concentration of DOX as 0.4 µM in cell media for 6 h and 24 h timepoints at 37 °C. Cells were collected by trypsin, washed twice with PBS and acquisition of cellular uptake was determined by flow cytometer BD LSRFortessa (BD Biosciences) by using PE channel (Ex_{max} 496 nm/Em_{max} 578 nm). All measurements were carried out in triplicates, results were analysed by Flowing Software 2.0. Gate was defined for live cells only; 20000 cells were recorded per sample. Fluorescence intensity of stocks (drug and nanoparticles) were measured by Thermofisher Varioskan plate reader for same Ex/Em values and results were normalized for cellular uptake comparison. Main fluorescence intensity of control cells was proportioned with the results to achieve uptake efficiency.

2.7.4. Doxorubicin localization by confocal microscopy

Evaluations of drug and nanoparticle localization in cells were determined by confocal microscopy. Cells were grown on coverslips ($15x10^4$ cells/sample) overnight in 6 well plates. The medium was replaced by solutions of DOX, PTX, DOX+PTX and nanoparticles (0.4 µM), respectively. After 1h, 6h and 24h timepoints, cells were rinsed with PBS, fixed with 4% PFA and sample was mounted using VECTASHIELD® with DAPI for microscopy. Zeiss LSM780 confocal microscopy (Plan-Apochromat 100x/1.40 Oil DIC), oil objective and Zen 2010 software consisting setup was used for imaging. Detection of DAPI was performed with 405 nm laser excitation and 450-500 nm emission. Argon laser 488 excitation was utilized for doxorubicin and emission was collected at 530-600 nm.

2.8. Ex vivo red blood cell hemolysis assay

Intravenous injection compatibility was investigated by ex vivo hemolysis assay as described by Evans et al.[33] Briefly, 5 ml of blood was obtained from a healthy anonymous human donor according to ethical requirements and drawn directly into Na_2EDTA coated tubes (1.6 mg/ml) to prevent coagulation. Full blood was centrifuged at 500xg for 5 min and haematocrit and plasma levels were marked on the tube. Red blood cells were washed by replacing plasma with 150 mM NaCl solution until the original plasma level. Cells were mixed gently and centrifuged at 500xg for 5 min. Red blood cells were washed twice with NaCl solution, and once with PBS thereafter diluted 50 times in PBS. Stock solutions of DOX, PTX, DOX+PTX and DOX-S-S-PTX were prepared in DMSO at x1000 the desired concentration to be tested, to eliminate the toxic effect of DMSO. 1 µL of stock solution was added in 1 ml red blood cell suspension and incubated at 37◦C for 24h. For positive control, 1% final concentration of Triton-X100 and for negative control 0.1% final concentration of DMSO was used. After incubation, cells were centrifuged at 500xg for 5 min, 200 µL supernatant was collected from each sample and absorbance of haemoglobin was measured by Varioskan plate reader at 500 nm. Experiment was done with triplicates and %hemolysis was calculated accordingly.

$$\%\text{Hemolysis} = \frac{\text{Abs sample} - \text{Abs negative control}}{\text{Abs positive control} - \text{Abs negative control}} \text{x}100$$

2.9. Modelling

To demonstrate that the prodrug itself has no or negligible therapeutic effects until it is break down into daughter drugs PTX-SH and DOX-SH, docking simulation was also carried out. The protein structures (PDB code: 1JFF and 1D12) was prepared through the Protein Preparation Wizard panel[34] to assign atom type and side chain protonation states before use. Molecular modelling suite Glide_XP[35] was use to predict the binding affinity of PTX-SH and DOX-SH by defining a 10 Å of empirical box localized at the centroid of PTX or DOX in complex structures.

3. Results and discussion

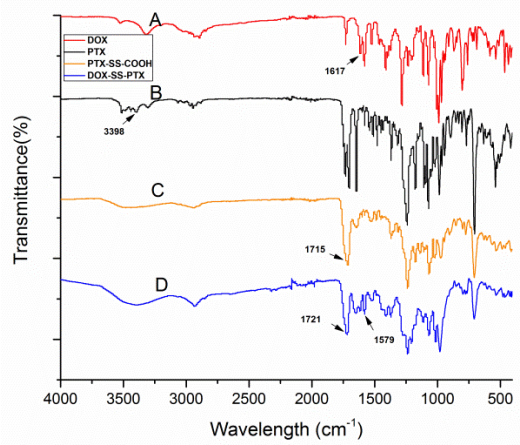

Fig. 3. FTIR spectra of (A)DOX.HCl; (B) PTX; (C)PTX-S-S-COOH; (D) DOX-S-S-PTX

3.1 Characterization of DOX-S-S-PTX

The FTIR spectra of DOX, PTX, PTX-S-S-COOH and DOX-S-S-PTX are presented in Fig. 3. As seen in the spectra of DOX·HCl (Fig. 3A), the peak at 1617 cm-1 is assigned to the -NH2 group bending vibration of DOX.[36, 37] The characteristic -OH stretching vibration peaks of PTX (Fig. 3B) of are at 3398 cm^{-1}.[38] The intense peak was observed at 1715 cm^{-1} (Fig. 3C), which is due to the absorption of C=O carboxylic acid. In theory, one equivalent DTPA bearing two carboxylic acid groups can possibly react with two stoichiometric equivalent PTX to give the PTX dimmer PTX-S-S-PTX. During our experiments, the yield of 10% PTX dimmer in maximum was detected while at least 80% yield of desired PTX-S-S-COOH was recovered by following Yin et al suggested a synthetic route[28]. To completely avoid unwanted dimmer product PTX-S-S-PTX, DTPA was dehydrated by reflux in methylene chloride at 70°C to get cyclic anhydride DTDPA at first, then the DTDPA react with PTX to obtain only monomeric PTX-S-S-COOH as the main product. This result is consistent with the report of cyclic succinic anhydride whose reaction with propargyl alcohol[39] and β-cyclodextrin[40] to give carboxylic acid terminated products. After the amide coupling reaction between PTX-S-S-COOH and DOX·HCl, the $-NH_2$ bending vibration peak disappears while the new peaks at 1721 cm^{-1} and at 1579 cm^{-1} are presented in Fig. 3D, which are attributed to the C=O stretching and -NH- bending vibration, individually. The above results indicate the successful synthesis of DOX-S-S-PTX.

^{1}H NMR of DOX-S-S-PTX and its intermediate products are shown in Fig. 4. As seen in Fig. 4A, the -COOH peak of DTDP is at d 12.35 ppm. After the refluxing in acetyl chloride, the -COOH peak of DTDP disappeared in Fig. 4B, suggesting the formation of DTDPA.

In addition, the thermogravimetric analysis shows the melting point of DTDP is 153-155 °C, and 65-70 °C for DTDPA. A dramatic change of melting points between DTDP and DTDPA also demonstrate the successful synthesis of DTDPA. The reaction of DTDPA and PTX is confirmed by the formation of an ester bond. The methylene ($-CH_2-CH_2-$) peak of DTDPA at δ 2.87 ppm and 2.61 ppm appear in both DTDPA and PTX-S-S-COOH spectra (Fig 4B and D).

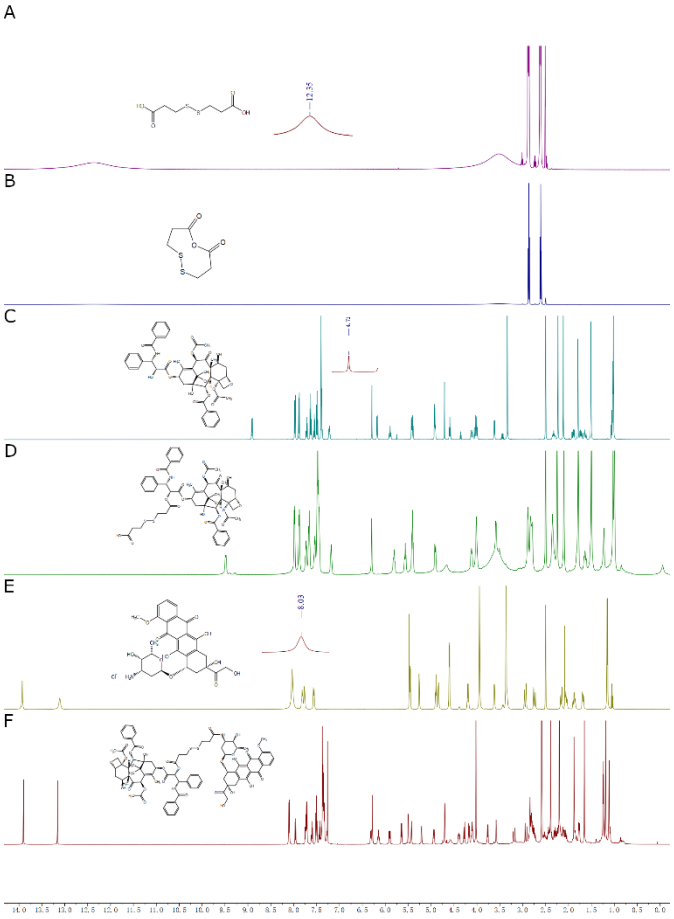

Fig. 4. ^{1}H NMR spectra of (A) DTDP in DMSO-d_6; (B) DTDPA in $CDCl_3$; (C) PTX in $CDCl_3$; (D) PTX-S-S-COOH in DMSO-d_6; (E) DOX in DMSO-d_6; (F) DOX-S-S-PTX in DMSO-d_6.

The aromatic protons peaks of PTX is at 7.25-8.25 ppm, 1.0-2.5 ppm for acetyl and methyl protons (Fig 4C). Among all hydroxyl groups in PTX, the activated DTPA (DTDPA) prefers to react with the hydroxyl group of PTX linked with C-2' to form the ester bond. The comparison of the 1H NMR spectra of PTX (Fig. 4C) and COOH-S-S-PTX (Fig. 4D) shows that the -OH peak at δ 4.71 ppm in PTX disappeared in Fig. 4D but the -COOH peak of COOH-S-S-PTX appear at 9.49 ppm; Furthermore, proton peak from 2.80 to δ 2.90 ppm shows the methylene(-CH_2-CH_2-S-S) peak of DTPA. The HRMS spectra of the product give the mass of 1044.3259 ([M-H]$^-$ in Fig. S3 A), together with suggested the desired molecules obtained.

Fig. 4E and F are the 1H NMR spectra of DOX and DOX-S-S-PTX respectively. Among all functional groups in DOX, the -NH_2 of daunosamine is the most suitable position for the modification of structure. As seen in Fig. 4E the -NH_2 peak of DOX is at 8.03 ppm. After the reaction of DOX with COOH-S-S-PTX, the -NH_2 peak disappeared in Fig. 4F. Furthermore, the -COOH of COOH-S

S-PTX is at 9.49 ppm, which also disappeared in Fig. 4F. In addition, observed mass of 1593.4638 $[M+Na]^+$ from HRMS spectra also suggested the successful conjugation of COOH-S-S-PTX with DOX into prodrug DOX-S-S-PTX.

3.2 The morphology, size and size distribution of the DOX-S-S-PTX nanoparticles

The intrinsic amphiphilicity of DOX-S-S-PTX prodrug favours itself to self-assemble into nanoparticles in the aqueous environment, which was demonstrated by both bulk method and microfluidics platform. However, bulk approach fails to give ideal results. As shown in Table S1 the smallest particle obtained is about 350.1 nm which is beyond the empirical particle size suitable for cellular uptake of no large than 200 nm. In general, both the size and polydispersity properties of bulk methods made particles are significantly deteriorated as compared with microfluidics devices. Using microfluidics devices, the effects of concentration prodrug and inner: outer (I: O) fluid flow on the characteristics of DOX-S-S-PTX nanoparticles were investigated to optimize the formulation. The morphology and size of DOX-S-S-PTX nanoparticles are shown in Fig. 5. The size, size distribution and ζ-potential of the nanoparticles were measured by DLS. At fixed I: O fluid flow of 2:40, changing the concentration of prodrug in inner flow lead to particle size and PDI variation (Fig. 5A, B). At the lowest DOX-S-S-PTX of 1 mg/ml, the average particle size of 99.04 nm (Fig. 5A) and the polydispersity index (PDI) of 0.106 (Fig. 5B) were achieved. The increased prodrug concentration barely affects the average size of nanoparticles but deteriorate the uniformity (Fig. 5B). When increasing DOX-S-S-PTX from 2 to 3mg/ml, the particle size enlarged to 181.9 nm but improved polydispersity (PDI of 0.084). More concentrated inner fluid payload up to 4 mg/ml worsened the characteristics

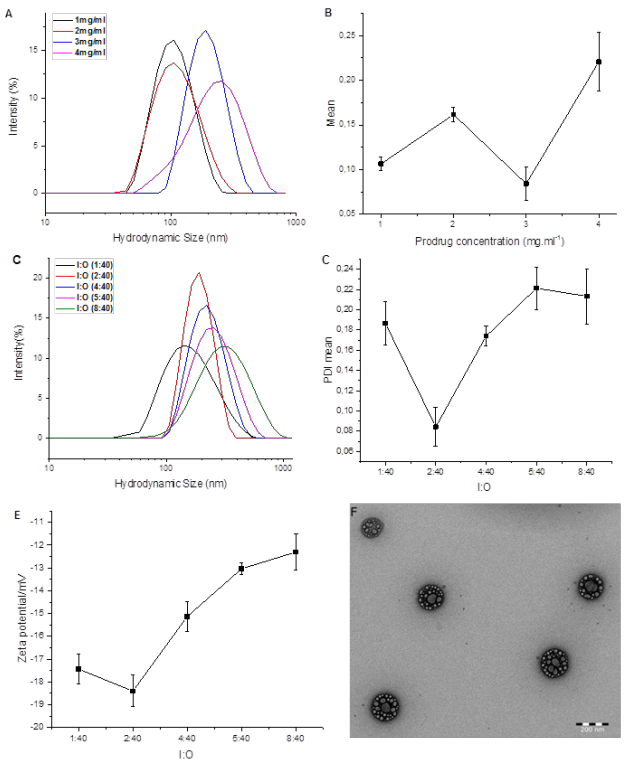

Fig.5 The morphology and size of DOX-S-S-PTX nanoparticles. (A) Hydrodynamic size and (B) PDI at different DOX-S-S-PTX prodrug concentration with fixed inner:outer (I:O) flow at 2:40 ml/h; (C)

Hydrodynamic size, (D) PDI at different inner:outer (I:O) flow and (E) ζ-potential at 3 mg/ml with DOX-S-S-PTX of 3mg/ml; (F) TEM of DOX-S-S-PTX nanoparticles with inner:outer (I:O) flow at 2:40 ml/h at 3 mg/ml with DOX-S-S-PTX of 3mg/ml.

of as-prepared nanoparticles, especially the PDI. Similarly, the physicochemical characteristics of the prodrug particles are also I: O fluid flow dependent. The average size of the DOX-S-S-PTX nanoparticles at I: O fluid flow = 1:40 is 147.2 nm (Fig. 5C) with the PDI of 0.187 (Fig. 5D) at fixed DOX-S-S-PTX prodrug concentration of 3mg/ml, while the average size is 181.9 nm (Fig. 5C) with the PDI of 0.084 (Fig. 5D), therefore is monodisperse when I: O = 2:40. The increased PDI at lowest I:O fluid flow (1:40) indicates possible aggregation of already formed small nanoparticles due to the slow mixing of inner and outer fluid.[41] At I:O of 4:40, both particle average size and size distribution increase to 220.9 nm 0.174. Further increase of inner fluid flow deteriorate the particles size and PDI up to 274.6 nm and 0.22 comparing to 2:40 ratio. This is because the increased inner fluid flow leads to the formation of microvortices which enhance the average mass transfer rates between inner and outer fluid flow, therefore accelerate the prodrug precipitation and more likely to form big sized nanoparticles. The ζ-potential of prepared prodrug nanoparticle is also varied (Fig. 5E) with the fluctuation of I: O fluid flow. At I: O fluid flow = 2:40 ζ-potential of the nanoparticles is about -18.5 mV, demonstrating the most stable product against aggregation in the current experiment.

It is generally suggested that nanoparticles with a size of 10-200 nm can passively accumulate in tumour cells via the EPR effect.[42, 43] Therefore, the fluid flow I:O= 2:40 and 3 mg/ml DOX-S-S-PTX prodrug concentration inner fluid were applied to inner fluid to fabricate as-prepared DOX-S-S-PTX for passive delivery to tumour cells. As shown in Fig. 5 F, the transmission electron microscopy (TEM) nanoparticles images demonstrate the uniform size of prodrug nanoparticles which are spherical and porous with centred large pores are surrounded by multiple smaller ones. The regular shape and hollow structure of particles may indicate the mechanical property of the particles which are made of DOX-S-S-PTX prodrug.

3.3 In vitro release of DOX from the DOX-S-S-PTX nanoparticles

The in vitro release profiles of the DOX-S-S-PTX nanoparticles in the absence and presence of DTT are shown in Fig. 6A. The accumulative release level of DOX from the nano-preparation of DOX-S-S-PTX prodrug show no difference in the first 10 h with and without DTT. The possible explanation is that both amide bond hydrolysis and disulfide bond breakage are involved in this process. In the beginning, it is not easy for the DTT to penetrate prodrug nanoparticle since hydrophilic DOX form the outer layer of nanoparticles. Therefore, the DOX predominately get released by hydrolysis of the amide bond in the nanoparticle of prodrug up to 40.9% at the PBS solution. After 10 h, the DTT can easily approach the disulfide bond in the prodrug nanoparticles due to swelling effect. DOX can now be released by breaking the disulfide bond by DTT. Nevertheless, the release profiles of samples with and without DTT scientifically differ after 10 h. When DTT is not charged, the concentration of DOX remains unchanged, indicating no further DOX molecules are released.

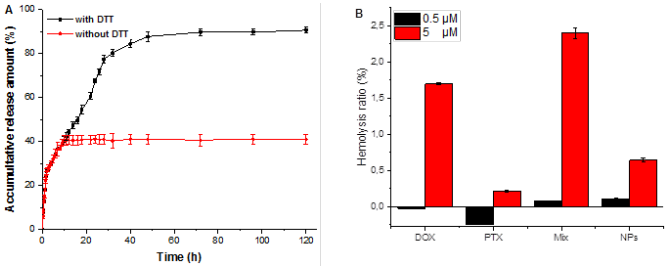

Fig. 6. (A) The in vitro release of DOX from DOX-S-S-PTX; (B) The hemolytic ratio of DOX-S-S-PTX nanoparticles.

On the contrary, for the sample with DTT DOX molecules continues to release until 72 h, and give 89.7% of an accumulative level, suggesting the disulfide bond damage contributes to about 50% of DOX release from DOX-S-S-PTX nanoparticles. The DOX release profile agreed with the report of mPEG-S-S-PTX micelles behaviour under the similar experimental conditions.[44] However, the in vitro release profiles of PTX (Fig. 6A) is not coincident with DOX since only 1.5% not a corresponding amount of PTX was detected. This is because the poor solubility prevents PTX being in aqueous PBS, while the liquid chromatographic method cannot monitor unsolved PTX. It is possible to introduce surfactant such Tween 80 to the experimental buffer to generate homogeneous PTX suspension. But the concern of surfactant may also increase the dissociation of prodrug molecules from prodrug nanoparticles alarm us not to do so.

3.4 The haemolytic test of the DOX-S-S-PTX nanoparticles

The haemolytic test was carried out to investigate the safety and suitability of the fabricated DOX-S-S-PTX prodrug nanoparticles for intravenous injection. The result of the haemolytic test of NPs, DOX, PTX, a mixture of DOX and PTX are shown in Fig. 6B. The haemolytic ratio of DOX-S-S-PTX nanoparticles at a concentration of 0.5 and 5 μM are all lower than 1%, suggesting that the NPs cannot cause red blood cell lysis.[45] In particular, at a higher concentration of 5 μM, NPs is safer than DOX alone and the combination since they triggered two to three folds higher haemolytic ratio. Therefore, the results show that our as-prepared prodrugs NPs are biocompatible for intravenous injection.

3.5 In vitro cytotoxicity and cell apoptosis

The cell viability of free drugs (DOX, PTX, DOX+PTX) and prodrug NPs was investigated with the WST-1 assay for MDA-MB-231, MDA-MB-231/ADR and MEF cells. The time points 24 h and 48 h were chosen for this study. Fig. 7 demonstrate that both free drugs reduce the viability of MDA-MB-231, MDA-MB-231/ADR and MEF cells. However, prodrug NPs have selective inhibition regarding cancer cells, while they do not alter the cell viability of healthy cells (Fig.7 E and F). In terms of free DOX, PTX, DOX+PTX mixture and prodrug NPs, dose-dependent manner was coherently observed in the cell proliferation inhibition. Besides, the 48 h inhibition ratio was higher than that of 24 h. These observations indicate that free DOX, PTX, NPs have time-dependent and concentration-dependent cytotoxic effects on cancer cells, but no effects were exerted to MEF cells by NPs. Fig.7 C and D suggested that the inhibition ratios of prodrug NPs

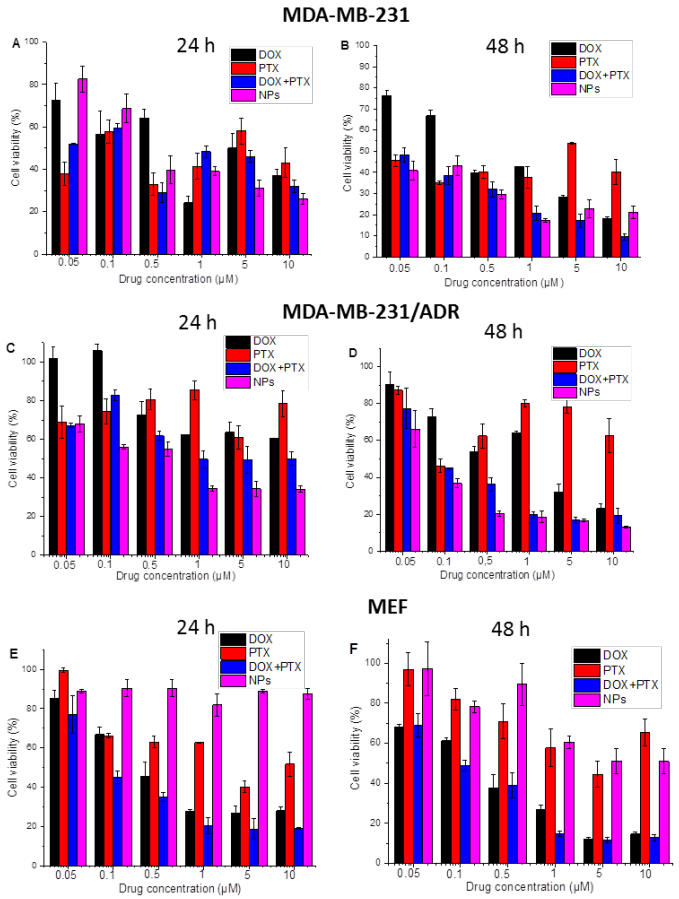

Fig. 7 Cytotoxicity of DOX, PTX, DOX+PTX mixture and NPs. MDA-MB-231 cells incubated for (A) 24 h, (B) 48 h, MDA-MB-231/ADR cells incubated for (C) 24 h, (D) 48 h, MEF cells incubated for (E) 24 h, (F) 48 h.

to drug resistant cancer cells were higher than for free DOX, PTX and physical mixture of DOX and PTX, implying faster NPs uptake and synergism of DOX and PTX may play the role.

3.6 Cellular uptake

The cellular uptake of DOX, DOX+PTX and prodrug NPs with MDA-MB-231, MDA-MB-231/ADR and MEF cells were investigated by flow cytometry for 6 h and 24 h time points. As illustrated in Fig. 8A and 8B, NPs exhibited poor uptake on healthy cells, whereas higher uptake was observed for free drugs, therefore NPs have the potential to eliminate possible side effects. PTX incorporation does not affect cellular uptake of DOX. In all tested cell lines, the uptake of NPs is lower comparing to free drugs, but faster since not drastic difference was observed between 6h and 24 h, implying the cellular uptake of NPs can quickly equilibrate. The lower NPs uptake is consistent with Cho's report,[46] which could be as a result of the negativity of NPs surface ζ-potential since the cell membrane is negatively charged[47] due to phospholipids bilayer structure, hence isoelectric charge repulsion prevents NPs from cell internalization. However, it was also reported that negatively charged particles had more cellular uptake than cationic particles. So it is suggested that the surface charge of nanoparticles is not the only affecting factor for their cellular uptake, yet hydrophobicity is equally important.[48, 49] In our as-prepared prodrug NPs, hydrophilic DOX tends to deploy on the surface, therefore such hydrophilic DOX "mask" may deteriorate the NPs pass of NPs into hydrophobic cell membrane.[50]

DOX is a fluorescent drug localizes in the nucleus as mechanisms of anticancer action,[51] which enables the microscopy imaging of nuclear localization. The result of the nuclear internalization of DOX was investigated by confocal fluorescence microscopy and images of the prodrug NPs and free drugs with MDA-MB-231, MDA-MB-231/ADR and MEF cells for 6 h and 24 h (in Fig. 8B and Fig. S45) are shown. For MDA-MB-231 and MDA-MB-231/ADR cells, DOX can already be detected in the nucleus after 1 h of incubation for free

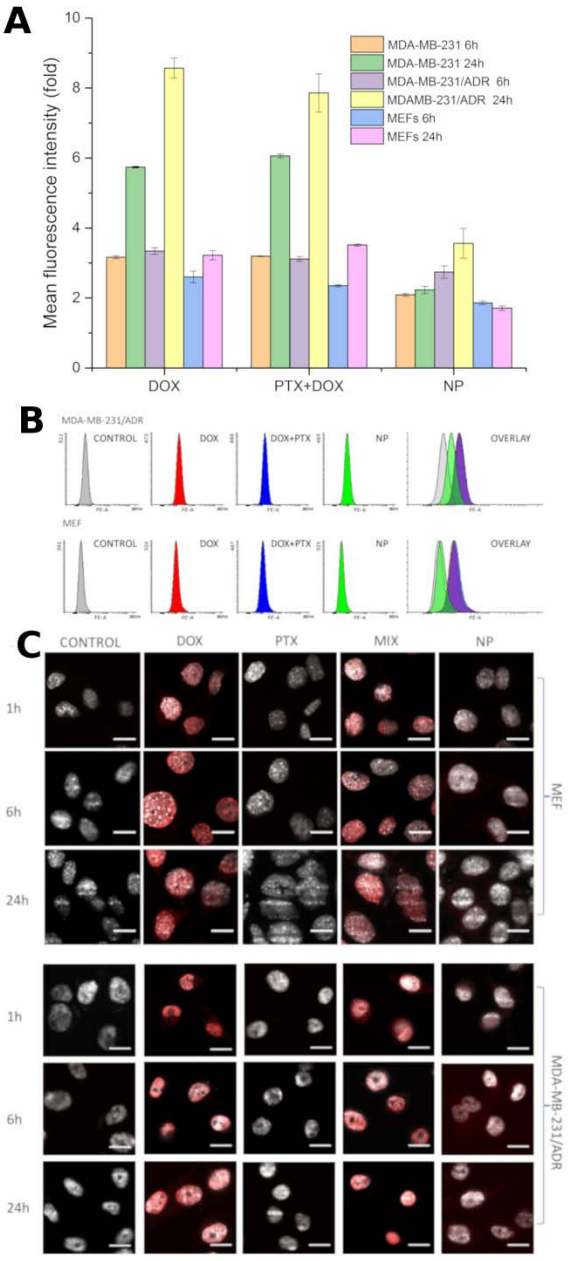

Fig.8 The fluorescence microscopy images and flow cytometry of cellular uptake of DOX, PTX, DOX+PTX and prodrug NP. (A) Mean fluorescence intensity of drug; (B) Flow cytometry of uptake in MDAMA-231-DOX and MEF cells and (C) Fluorescence microscopy images with Scale bar 10 μm.

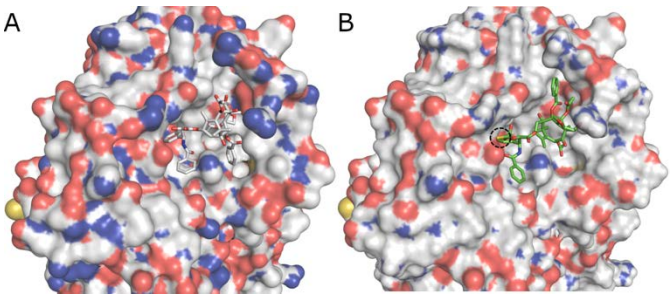

Fig. 9 The complex of β-tubulin with (A) PTX (PDB file: 1JFF[53]) and (B) predicted binding modes of PTX-SH. The dashed circle highlighted the thiol moiety.

drug and prodrug NPs. The fluorescence can still be detected on 6 h and 24 h timepoints which proves the efficacy of prodrug NPs. It is clearly seen that the intensity of NPs is less when compared with free drug, and this suggests the fluorescence intensity loss could be due to prodrug conjugation. Regardless of the incubation timepoints (Fig. 8A), the fluorescence intensity of DOX in MEF cells treated with NPs had no obvious change whereas free DOX and DOX+PTX internalization was observed, which suggests the NPs mainly accumulate in MDAMA-231/ADR cells hence eliminating possible unwanted side effects.

3.7 In silico simulation

PTX with brand name Taxol is a cytoskeletal drug that targets β tubulin to interfere with the cell microtubule assembly-disassembly process to an arrested cell in the G2/M-phase cycle and ultimately lead to cell apoptosis.[52] It has been proposed that the release of PTX from mPEG-SS-PTX conjugated micelles can be achieved through both the esterase induced hydrolysis and GSH related disulfide breakdown.[44] The ester bond hydrolysis leads to native drug PTX which we believe it should go to target macromolecules to enable the function. When the reduction of disulfide bond GSH gave PTX-CH_2-CH_2-SH which we believe it should bind to PTX's biological target alike since only short spacer (-CH_2-CH_2-SH) was introduced. To confirm it, molecular docking was performed. Fig. 9 A represented the binding of PTX in β tubulin. In parallel, the docked PTX-CH_2-CH_2-SH to β tubulin with highest docking score was shown in Fig. 9B, demonstrating very similar binding pose with PTX. The framework of PTX-CH_2-CH_2-SH localizes into the binding pocket of PTX while the spacer (-CH_2-CH_2-SH) moiety point to the solvent (highlighted by dash circle). Another half of prodrug DOX-CH_2-CH_2-SH was also docked to the therapeutic target of DOX DNA topoisomerase II.[54] The similar binding pose with DOX to the biological target was also obtained (the data is not showed). There is no doubt the reduced products PTX-CH_2-CH_2-SH and DOX- CH_2-CH_2-SH can be enzymatically hydrolyzed into PTX and DOX by esterase and proteases individually.

Conclusions

In this work, we propose a new drug delivery system based on PTX-S-S-DOX prodrug by the conjugation of PTX and DOX through a disulfide bond. Due to the of hydrophobicity balance of carefully selected components, obtained DOX-S-S-PTX amphiphilic prodrug self-assembled into NPs through microfluidics-tailored nanoprecipitation. The size of as-prepared NPs can be tuned by adjusting the inner: outer flow and concentration of prodrug in the inner solvent channel. The obtained NPs are stable and safe. The disulfide bond in the DOX-S-S-PTX conjugate can be broken in the reducing environment of tumour cells, leading to the controlled release of two daughter drugs simultaneously. The prepared NPs inhibit the cancer cells in the dose- and time-dependent manner but not healthy MEF cells. Although less NPs was untaken by this uptake is quicker comparing to free drugs. NPs internalize into diseased cells with large quantity but less in healthy ones, implying this prodrug nanoprecipitation formulation are advantageous over free drug administration in terms of minimizing drug side effects.

Conflicts of interest

Authors declare no conflicts of interests.

Acknowledgements

This work was supported by Distinguished Clinical Investigator Grant of Jiangsu Province, China (Grant No. JSTP201701), Academy of Finland (Grant No. 297580) and Sigrid Jusélius Foundation (decision no. 28001830K1). Authors are thankful to Peiru Yang and Fang Chen for donating the DOX resistant cell line, Dhayakumar Rajan Prakash to reshape the Fig.1 of this manuscript. Gunilla Henriksson is kindly acknowledged for helping hemolysis study.

Notes and references

1. H. K. Weir, R. N. Anderson, S. M. C. King, A. Soman, T. D. Thompson, Y. Hong, B. Moller and S. Leadbetter, *Preventing chronic disease*, 2016, **13**.
2. K. Curtius, N. A. Wright and T. A. Graham, *Nature Reviews Cancer*, 2018, **18**, 19.
3. P. A. Pesavento, D. Agnew, M. K. Keel and K. D. Woolard, *Nature Reviews Cancer*, 2018, 1.
4. J. Dubach, C. Vinegoni, R. Mazitschek, P. F. Feruglio, L. Cameron and R. Weissleder, *Nature communications*, 2014, **5**, 3946.
5. F. Kamangar, G. M. Dores and W. F. Anderson, *Journal of clinical oncology*, 2006, **24**, 2137-2150.
6. J. Rautio, N. A. Meanwell, L. Di and M. J. Hageman, *Nature Reviews Drug Discovery*, 2018.
7. D. Platel, S. Bonoron-Adele, R. Dix and J. Robert, *British journal of cancer*, 1999, **81**, 24.
8. M. Kapoor and R. A. Siegel, *Molecular pharmaceutics*, 2013, **10**, 3519-3524.
9. J. Hulla, S. Sahu and A. Hayes, *Human & experimental toxicology*, 2015, **34**, 1318-1321.
10. Y. Ma, Q. Mou, X. Zhu and D. Yan, *Materials Today Chemistry*, 2017, **4**, 26-39.
11. N. T. Chi, N. M. Triet and D. M. Chien, 2009.
12. M. Iqbal, N. Zafar, H. Fessi and A. Elaissari, *International journal of pharmaceutics*, 2015, **496**, 173-190.
13. D. Quintanar-Guerrero, M. de la Luz Zambrano-Zaragoza, E. Gutiérrez-Cortez and N. Mendoza-Muñoz, *Recent patents on drug delivery & formulation*, 2012, **6**, 184-194.
14. B. Nagavarma, H. K. Yadav, A. Ayaz, L. Vasudha and H. Shivakumar, *Asian J. Pharm. Clin. Res*, 2012, **5**, 16-23.
15. M. Beck-Broichsitter, E. Rytting, T. Lebhardt, X. Wang and T. Kissel, *European Journal of Pharmaceutical Sciences*, 2010, **41**, 244-253.

16. K. S. Yadav and K. K. Sawant, *Aaps Pharmscitech*, 2010, **11**, 1456-1465.
17. J. Xu, S. Zhang, A. Machado, S. Lecommandoux, O. Sandre, F. Gu and A. Colin, *Scientific Reports*, 2017, **7**, 4794.
18. E. Chiesa, R. Dorati, T. Modena, B. Conti and I. Genta, *International journal of pharmaceutics*, 2018, **536**, 165-177.
19. D. Liu, C. R. Bernuz, J. Fan, W. Li, A. Correia, J. Hirvonen and H. A. Santos, *Advanced Functional Materials*, 2017, **27**, 1604508.
20. D. Liu, H. Zhang, S. Cito, J. Fan, E. Mäkilä, J. Salonen, J. Hirvonen, T. M. Sikanen, D. A. Weitz and H. l. A. Santos, *Nano letters*, 2017, **17**, 606-614.
21. H. Hillaireau, N. Dereuddre-Bosquet, R. Skanji, F. Bekkara-Aounallah, J. Caron, S. Lepêtre, S. Argote, L. Bauduin, R. Yousfi and C. Rogez-Kreuz, *Biomaterials*, 2013, **34**, 4831-4838.
22. A. Gaudin, M. Yemisci, H. Eroglu, S. Lepetre-Mouelhi, O. F. Turkoglu, B. Dönmez-Demir, S. Caban, M. F. Sargon, S. Garcia-Argote and G. Pieters, *Nature nanotechnology*, 2014, **9**, 1054.
23. P. Huang, D. Wang, Y. Su, W. Huang, Y. Zhou, D. Cui, X. Zhu and D. Yan, *Journal of the American Chemical Society*, 2014, **136**, 11748-11756.
24. S. Lou, Z. Zhao, M. Dezort, T. Lohneis and C. Zhang, *ACS omega*, 2018, **3**, 9210-9219.
25. M. P. Gamcsik, M. S. Kasibhatla, S. D. Teeter and O. M. Colvin, *Biomarkers*, 2012, **17**, 671-691.
26. R. Ngoune, A. Peters, D. von Elverfeldt, K. Winkler and G. Pütz, *Journal of Controlled Release*, 2016, **238**, 58-70.
27. X. Zheng, Z. Li, L. Chen, Z. Xie and X. Jing, *Chemistry–An Asian Journal*, 2016, **11**, 1780-1784.
28. T. Yin, Q. Wu, L. Wang, L. Yin, J. Zhou and M. Huo, *Molecular pharmaceutics*, 2015, **12**, 3020-3031.
29. D. Liu, H. Zhang, E. Mäkilä, J. Fan, B. Herranz-Blanco, C.-F. Wang, R. Rosa, A. J. Ribeiro, J. Salonen and J. Hirvonen, *Biomaterials*, 2015, **39**, 249-259.
30. D. Liu, S. Cito, Y. Zhang, C. F. Wang, T. M. Sikanen and H. A. Santos, *Advanced Materials*, 2015, **27**, 2298-2304.
31. B. Herranz-Blanco, E. Ginestar, H. Zhang, J. Hirvonen and H. A. Santos, *International journal of pharmaceutics*, 2017, **516**, 100-105.
32. W. Zhu, Y. Wang, X. Cai, G. Zha, Q. Luo, R. Sun, X. Li and Z. Shen, *Journal of Materials Chemistry B*, 2015, **3**, 3024-3031.
33. B. C. Evans, C. E. Nelson, S. Y. Shann, K. R. Beavers, A. J. Kim, H. Li, H. M. Nelson, T. D. Giorgio and C. L. Duvall, *Journal of visualized experiments: JoVE*, 2013.
34. G. M. Sastry, M. Adzhigirey, T. Day, R. Annabhimoju and W. Sherman, *Journal of computer-aided molecular design*, 2013, **27**, 221-234.
35. R. A. Friesner, R. B. Murphy, M. P. Repasky, L. L. Frye, J. R. Greenwood, T. A. Halgren, P. C. Sanschagrin and D. T. Mainz, *Journal of medicinal chemistry*, 2006, **49**, 6177-6196.
36. L. Chen, Y. Xue, X. Xia, M. Song, J. Huang, H. Zhang, B. Yu, S. Long, Y. Liu and L. Liu, *Journal of Materials Chemistry B*, 2015, **3**, 8949-8962.
37. D. Zhao, J. Wu, C. Li, H. Zhang, Z. Li and Y. Luan, *Colloids and Surfaces B: Biointerfaces*, 2017, **155**, 51-60.
38. G. Kathiravan, S. V. Raman, B. Rajangam and A. Rajasekar, *Journal of Analytical & Bioanalytical Techniques*, 2014, **5**, 1.
39. J.-H. Wang, C.-C. Cheng, Y.-C. Yen, C.-C. Miao and F.-C. Chang, *Soft Matter*, 2012, **8**, 3747-3750.
40. Y. Xi, Z. Luo, X. Lu and X. Peng, *Journal of agricultural and food chemistry*, 2017, **66**, 228-237.
41. Y. Kim, B. Lee Chung, M. Ma, W. J. Mulder, Z. A. Fayad, O. C. Farokhzad and R. Langer, *Nano letters*, 2012, **12**, 3587-3591.
42. N. Hoshyar, S. Gray, H. Han and G. Bao, *Nanomedicine*, 2016, **11**, 673-692.
43. E. Blanco, H. Shen and M. Ferrari, *Nature biotechnology*, 2015, **33**, 941.
44. D. Zhao, H. Zhang, S. Yang, W. He and Y. Luan, *International journal of pharmaceutics*, 2016, **515**, 281-292.
45. H. Wang, Y. Zhao, Y. Wu, Y.-l. Hu, K. Nan, G. Nie and H. Chen, *Biomaterials*, 2011, **32**, 8281-8290.
46. E. C. Cho, J. Xie, P. A. Wurm and Y. Xia, *Nano letters*, 2009, **9**, 1080-1084.
47. B. Chen, W. Le, Y. Wang, Z. Li, D. Wang, L. Ren, L. Lin, S. Cui, J. J. Hu and Y. Hu, *Theranostics*, 2016, **6**, 1887.
48. Z. Zhang, K. Van Steendam, S. Maji, L. Balcaen, Y. Anoshkina, Q. Zhang, G. Vanluchene, R. De Rycke, F. Van Haecke and D. Deforce, *Advanced Functional Materials*, 2015, **25**, 3433-3439.
49. A. Valsesia, C. Desmet, I. Ojea-Jiménez, A. Oddo, R. Capomaccio, F. Rossi and P. Colpo, *Communications Chemistry*, 2018, **1**, 53.
50. L. Lacerda, H. Ali-Boucetta, S. Kraszewski, M. Tarek, M. Prato, C. Ramseyer, K. Kostarelos and A. Bianco, *Nanoscale*, 2013, **5**, 10242-10250.
51. N. S. H. Motlagh, P. Parvin, F. Ghasemi and F. Atyabi, *Biomedical optics express*, 2016, **7**, 2400-2406.
52. N. C. Kampan, M. T. Madondo, O. M. McNally, M. Quinn and M. Plebanski, *BioMed research international*, 2015, **2015**.
53. J. Löwe, H. Li, K. Downing and E. Nogales, *Journal of molecular biology*, 2001, **313**, 1045-1057.
54. J. L. Nitiss, *Nature Reviews Cancer*, 2009, **9**, 338.